The Influence of the Silicon Content on the Formation of $Fe_{23}B_6$ Metastable Phases in $Fe_{65}Co_{11-x}B_{20}Si_xZr_2Hf_2$ Bulk Amorphous Alloys

MARCIN NABIAŁEK, BARTŁOMIEJ JEŻ, and KATARZYNA BŁOCH

This study aims to determine the effect of addition of a small quantity of Si on the formation of nanocrystalline structure in rapidly cooled Fe-Co-B alloys. As part of the work, the following alloys were produced using a method involving the forcing of each respective liquid alloy into a copper mold: $Fe_{65}Co_{11-x}B_{20}Si_xZr_2Hf_2$ (where: $x = 0$; 0.25; 0.5; 0.75; 1). Analysis of recorded X-ray diffraction patterns confirmed that a nanocrystalline structure was obtained in the alloys. The intensity of the diffraction reflections was found to change with changing Si content. The $Fe_{23}B_6$ crystalline phase was present in the volume of each alloy. This phase has soft magnetic properties. The presence of the $Fe_{23}B_6$ phase was confirmed by measurements of the magnetic polarization of saturation as a function of temperature.

https://doi.org/10.1007/s11661-020-05894-y

I. INTRODUCTION

SILICON is an important component of many materials used in electronics and electrical engineering. For example, it is widely used in the magnetic circuits of electric machines in the form of the so-called silicon steels (with Si contents of up to several percent, and low C content). These steels have very high values of saturation magnetization (up to 2T). However, they are characterized by low magnetic permeability values and significant losses on magnetization.[1]

These losses can be reduced by using an oriented structure with a suitable grain size. This affects the number and size of magnetic domains found in commonly used electrotechnical materials.

The above textured crystalline materials have been widely known for several decades. New materials are constantly being sought for which better magnetic properties can be obtained. This group of materials includes amorphous and nanocrystalline materials.[2] It should be recognized that the starting material is always an amorphous material and its further modifications affect its properties. In the first stage, this material can be annealed, then nanocrystallized (partial crystallization), and finally fully crystallized. Each of these materials, despite having the same chemical composition, has different magnetic properties. The reason for this is a different structure and other mechanisms governing their properties.

Amorphous and nanocrystalline alloys with good magnetic properties can be obtained by rapid quenching of a liquid alloy with a high Fe content.[3] A nanocrystalline material consists of an amorphous matrix and nanocrystalline grains. The amorphous matrix usually has slightly inferior properties compared with the nanocrystalline grains.[4, 5] Such a material can be called a magnetic composite.

The amorphous matrix should be almost zero magnetostrictive material with moderate saturation magnetization and low coercive field. In the case where a small amount of nanocrystalline grains is formed in the amorphous matrix, in addition to large dimensions (several dozen nanometers), the properties of this composite are poor. It should be noted that for the same chemical composition of the amorphous crystalline composite, a completely inverse relationship of properties may occur. For high content of the crystalline phase (over 70 pct) characterized by small grains (up to several nanometers), rapid softening of the alloy and an increase in its magnetization are observed.[6] The crystalline grains, distributed in the matrix, cause an increase in the overall saturation magnetization of the material, and, due to their size and distribution, they decrease the value of the coercive field—which in turn minimizes the loss of magnetization.[7]

There are various methods for obtaining nanocrystalline alloys. The most common is that of annealing amorphous precursors at temperatures close to the crystallization temperature of the alloy. A suitably

MARCIN NABIAŁEK, BARTŁOMIEJ JEŻ, and KATARZYNA BŁOCH are with the Department of Physics, Faculty of Production Engineering and Materials Technology, Czestochowa University of Technology, 19 Armii Krajowej Str., 42-200 Czestochowa, Poland. Contact e-mail: nabialek.marcin@wip.pcz.pl

Manuscript submitted January 16, 2020.
Article published online July 7, 2020

selected temperature and annealing time allows control of the nanocrystallization process.[8–10] This process involves the conglomeration of groups of atoms and the creation of energetically privileged areas—from which nuclei are formed, and, subsequently, the grains of the crystalline phases. Another way to obtain nanocrystalline material is pulsed laser heating of amorphous precursors. In this case, the laser beam power and irradiation rate should be carefully selected in order to obtain an appropriate quantity of energy per unit area in the amorphous material.[11, 12] From the point of view of time saving and simplification of the production process, it is advantageous to manufacture nanocrystalline alloys in a single-step process. The correct selection of manufacturing processes and the chemical composition of the alloy are of major importance. The influence of silicon on the formation of amorphous structure has already been quite well described. There are many studies related to alloys from the Fe-Si-B,[13–16] Fe-Co-B [17–20] and Fe-Zr-B [21–24] systems. However, there is no research on bulk rapidly-cooled alloys from the Fe-Co-B system, with a Si micro-additive; therefore, it was considered appropriate to carry out tests on such a group of alloys.

Samples of bulk rapidly-cooled alloys were produced, with the following chemical compositions: $Fe_{65}Co_{11-x}B_{20}Si_xZr_2Hf_2$ (where: $x = 0; 0.25; 0.5; 0.75; 1$). The aim of the work was to determine the effect of the addition of a small quantity of Si on the formation of nanocrystalline structure in rapidly-cooled alloys, and on the soft magnetic properties of the produced alloys.

II. METHODS AND MATERIALS

The chemical compositions of the alloys were selected on the basis of the criteria for producing amorphous alloys, as proposed by Inoue.[25] The main alloying components are characterized by negative mixing heat and contrasting lengths of atomic radii (Figure 1).

Silicon is characterized by negative heat of mixing with all of the other alloy components, therefore its addition may affect the alloy's ability to vitrify.[25]

Polycrystalline alloys, with the chemical compositions $Fe_{65}Co_{11-x}B_{20}Si_xZr_2Hf_2$(where: $x = 0; 0.25; 0.5; 0.75; 1$), were produced under an inert atmosphere in an arc furnace. The solidification of each alloy was preceded by the melting of a titanium getter, in order to obtain a high degree of atmospheric purity in the working chamber. Ingredients with a purity of greater than 99.9 pct were used to make the 5 g ingots. The ingots were subjected to both mechanical and ultrasonic cleaning, after which the alloy was divided into smaller pieces. The test samples were produced using a method involving the forcing of liquid alloy into a water-cooled copper mold.[27, 28] This method allows a cooling rate in the range of 10^{-1} to 10^3 K/s to be achieved. The samples were cast in the form of plates with the following dimensions: 10 mm × 5 mm × 0.5 mm. Each polycrystalline ingot in turn was placed in a quartz crucible at the top of a copper coil. The load was melted using eddy-current heating. Under argon pressure (at 800 hPa), the liquid alloy was drawn out, through a 1 mm diameter hole in a quartz crucible, into the copper mold. The resulting alloy samples were cleaned—both mechanically and using an ultrasonic cleaner. The resulting samples were subjected to structural tests using X-ray diffraction analysis. For this, a BRUKER D8 Advance X-ray machine, equipped with a CuKα lamp, was used. The samples were exposed for seven seconds per measuring step (0.02 deg). The X-ray diffraction measurement was carried out in the 2θ range from 30 to 100 deg. Identical mass samples were prepared for XRD tests. Specialized Match! Software was used to identify crystalline phases occurring in the volume of each of the produced samples. In addition, the average size of the crystallites was determined using the Scherrer relationship (1).[27]

$$D = (\lambda * K)/2_0 \cos\theta \qquad [1]$$

where: K—Scherrer shape coefficient ($K = 0.91$), λ—characteristic radiation wavelength, B_0—half-width in the middle of the peak intensity (the background was considered in the analysis), θ—Bragg angle.

The average grain size was estimated taking into account the peaks occurring for the following 2 theta angle values: $Fe_{23}B_6$: 43.66; 43.78; 41.05; 50.09; 37.29; 47.75; 50.87; 33.37; αFe: 44.64; 82.27).

The magnetic properties of the produced materials were measured using a Faraday balance (for the saturation magnetic polarization as a function of temperature, at 0.7 T of the external magnetic field strength) and a Lakeshore vibrating sample magnetometer (VSM—for the initial magnetization curve and the static magnetic hysteresis loops, in the range of 0 to 2 T of external magnetic field strength). Analysis of the initial magnetization curves, in the Holstein–Primakoff paraprocess region, allows the determination of a parameter describing the stiffness of the spin-wave (D_{spf}). The parameter D_{spf} is described by the following equation [29]:

$$D_{sp} = \frac{1}{3} S J_{ex}(a) a^2 z_m \qquad [2]$$

where S the spin value in the distance from the central atom, J_{ex} the local exchange integral, a the distance to the nearest–neighbor atoms, z_m the number of nearest–neighbour magnetic atoms.

III. RESEARCH RESULTS

Figure 2 contains X-ray diffraction images recorded for the $Fe_{65}Co_{11-x}B_{20}Si_xZr_2Hf_2$ alloys after solidification. A wide maximum (at 2θ angle of 40 to 50 deg), with clear narrow reflections, is noticeable on all X-ray diffraction patterns. The wide maximum indicates the presence of an amorphous matrix, and its shape is associated with the scattering of X-rays on randomly distributed atoms within the volume of the sample. Narrow peaks are associated with the presence of small grains, originating from crystalline phases. This shape of diffractogram is typical for nanocrystalline materials. Based on analysis of the X-ray diffraction patterns, it

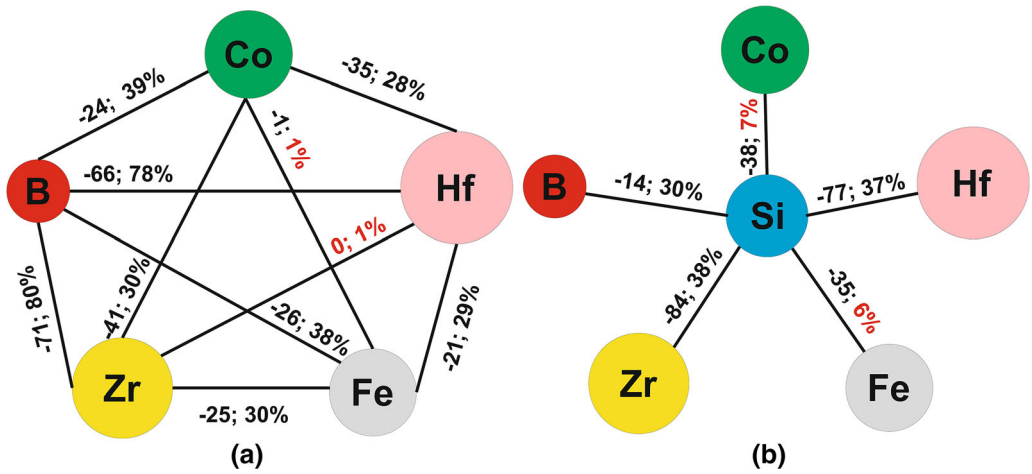

Fig. 1—Mixing heat for alloy components: (*a*) for alloy without Si addition and (*b*) for Si and other alloy components.

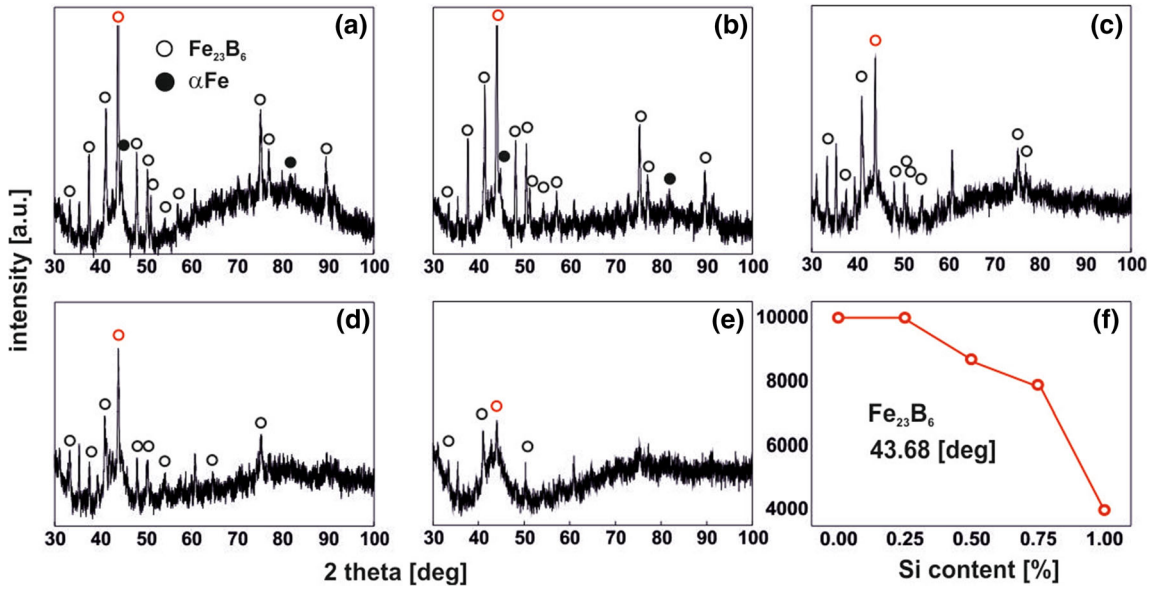

Fig. 2—X-ray diffraction images for the investigated alloys: (*a*) $Fe_{65}Co_{11}B_{20}Zr_2Hf_2$, (*b*) $Fe_{65}Co_{10.75}B_{20}Si_{0.25}Zr_2Hf_2$, (*c*) $Fe_{65}Co_{10.5}B_{20}Si_{0.5}Zr_2Hf_2$, (*d*) $Fe_{65}Co_{10.25}B_{20}Si_{0.75}Zr_2Hf_2$, (*e*) $Fe_{65}Co_{10}B_{20}Si_1Zr_2Hf_2$, (*f*) 100 ring intensity for $Fe_{23}B_6$ phase.

was found that the intensity for ring 100 decreases with the proportion of the Si additive (red hollow ring—main peak, Figure 2(f)). The addition of silicon has a significant effect on glass forming ability, even in very small quantities.[30] It is worth noting that, with a content of > 0.25 at. pct Si (Figures 2(a) and (b)), there is no crystalline phase αFe in the volume of the tested samples. In classical Fe-Si-B alloys with a Si content of 10 to 20 at. pct, a crystalline solution of solid silicon in iron is formed during the primary crystallization, while boron is distributed into an amorphous matrix.[31] This clearly means that the primary crystallization process is a diffusion controlled one. In the present study, a completely different group of materials is being investigated, *i.e.*, bulk amorphous materials, and a small addition of Si is being introduced as a structural stabilizer: 0.25, 0.5, 0.75, 1 at. pct. Fe phase crystals and borides by limiting the diffusion of atoms over further distances (Figure 3). Increasing the Si content hinders the growth of αFe phase crystals and borides by limiting the diffusion of atoms over longer distances (Figure 3).

Based on analysis of the X-ray diffraction patterns, three magnetic phases with soft magnetic properties were identified in the sample volume: an amorphous matrix and two crystalline phases: $Fe_{23}B_6$, αFe. The $Fe_{23}B_6$ crystalline phase has an identity period of around 1.2 nm [32] and has a Curie temperature in the range 648 to 662 K.[33] In contrast, the crystalline phase αFe has, respectively: an identity period of 0.286 nm and

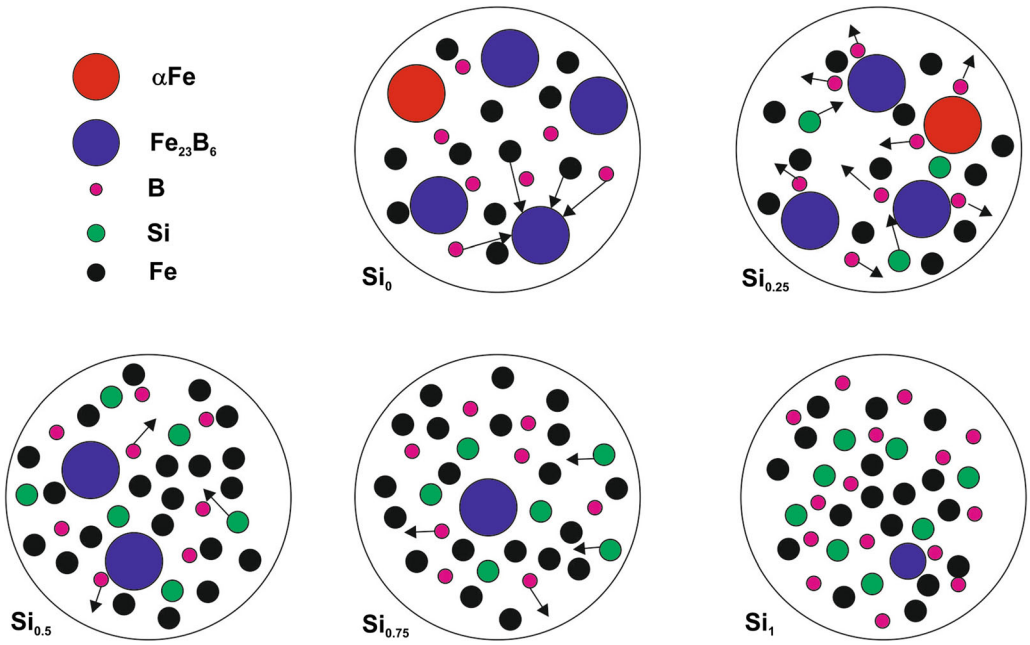

Fig. 3—Mechanism of blocking crystalline phase growth in the tested alloys.

a Curie temperature of 1041 K. Based on the registered X-ray diffraction patterns, an analysis of lattice parameters of the identified crystalline phases was performed (Table I). It turns out that with increasing Si content in the alloy, lattice parameters for phases αFe and $Fe_{23}B_6$ take lower values. As many papers indicate,[34, 35] fine grains of the αFe phase in an amorphous matrix, usually between 3 and 18 nm in size, enhance soft magnetic properties and reduce the coercive field value. These properties have been well described by Herzer, in models of so-called random anisotropy.[6] It is obvious that the effect resulting from the formation of crystal grains in the amorphous matrix is the reduction of certain elements that are absorbed by the forming phases. This disturbs the chemical composition of the amorphous matrix and increases chemical disorder. Changes in the magnetic polarization of saturation, as a function of temperature, reflect the described chemical composition disturbances in the amorphous matrix. Figure 4 contains magnetic saturation polarization curves, as a function of temperature. The measurements were carried out over the range from room temperature to up to 850 K. The height of the magnetic polarization curve, as a function of temperature, is affected by the distance between neighboring magnetic atoms that interact with each other. The smaller the distance between magnetic atoms, the higher the peak of the thermomagnetic curve μ0M (T), as shown in Figure 4. For all of the investigated alloys, only one mild inflection is visible within the examined range; this effect is associated with the transition of the amorphous magnetic phase from the ferro- to paramagnetic state. It should be emphasized that, in addition to the amorphous matrix, grains of the crystalline phases αFe and $Fe_{23}B_6$ are present in the sample volume (Figure 4(a) and (b)) and in the other samples, grains of the $Fe_{23}B_6$ crystalline phase (Figure 4(c) to (e)). If the magnetic saturation polarization does not reach values close to zero, it means that, in addition to the contribution of the amorphous matrix to the magnetic saturation polarization as a function of temperature, a contribution is observed from magnetic periodic crystallographic systems. Such a structure can be called a magnetic composite, made of an amorphous matrix and grains of crystalline phases. It is possible that interacting magnetic atoms from the amorphous matrix will be separated by crystal grains. As a result, as mentioned above, this can affect the curve value as well as the Curie temperature. Just above 800 K, an increase in magnetic saturation polarization is visible. Due to the nature of the maximum and the temperature range, these details should be associated with the crystallization of the amorphous matrix.

For alloys that meet Heisenberg's assumptions, it is possible to determine the Curie temperature using the critical factor $\beta = 0.36$ (inserts in Figure 4). Based on analysis of the $(\mu_0 M/\mu_0 M_S)^{1/\beta}$ curves, the Curie temperature was determined for magnetic phases present in the volume of tested samples—in the temperature range up to 850 K. Depending on the alloy, the Curie temperature fluctuates slightly, and this may be related to the metastable nature of the crystalline phase formed, changes in the short-range chemical order, and stresses in the amorphous matrix arising during the solidification process of the alloy. The change in the Curie temperature value can be explained by the change in the lattice parameters of the crystal phases αFe and $Fe_{23}B_6$. If Si atoms are dissolved in $Fe_{23}B_6$ lattice, it is likely they change the interatomic distance, which strongly changes the exchange energy and, subsequently, the values of T_C (Table II). An assessment of the influence of magnetic phases on the trajectories of thermomagnetic curves was carried out. Additionally, the influence can be

Table I. Estimated Average Grain-Sizes and Lattice Parameter of Identified Crystalline Phases in the Produced Alloys

Alloy/Phase	αFe			$Fe_{23}B_6$	
	Average Grain-Sizes (nm)		Lattice Parameter (nm)	Average Grain-Sizes (nm)	Lattice Parameter (nm)
$Fe_{65}Co_{11}B_{20}Zr_2Hf_2$	13.0		0.2872	28.9	1.0763
$Fe_{65}Co_{10.75}B_{20}Si_{0.25}Zr_2Hf_2$	18.9		0.2861	32.2	1.0745
$Fe_{65}Co_{10.5}B_{20}Si_{0.5}Zr_2Hf_2$	—		—	24.4	1.0732
$Fe_{65}Co_{10.25}B_{20}Si_{0.75}Zr_2Hf_2$	—		—	21.3	1.0712
$Fe_{65}Co_{10}B_{20}Si_1Zr_2Hf_2$	—		—	8.5	1.0703

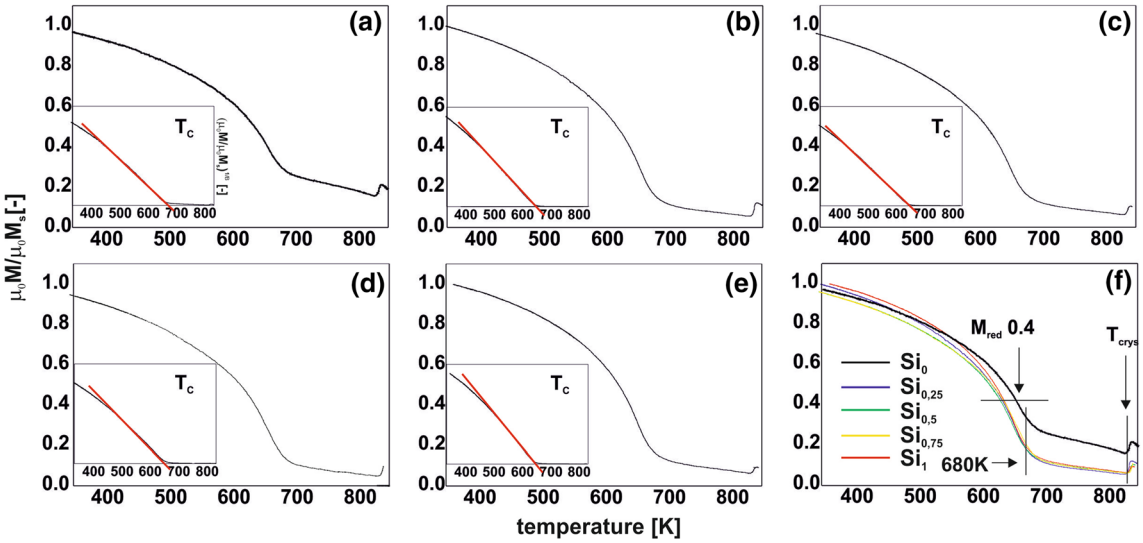

Fig. 4—Magnetic saturation polarization curves, as a function of temperature, measured for the investigated alloys: (*a*) $Fe_{65}Co_{11}B_{20}Zr_2Hf_2$, (*b*) $Fe_{65}Co_{10.75}B_{20}Si_{0.25}Zr_2Hf_2$, (*c*) $Fe_{65}Co_{10.5}B_{20}Si_{0.5}Zr_2Hf_2$, (*d*) $Fe_{65}Co_{10.25}B_{20}Si_{0.75}Zr_2Hf_2$, (*e*) $Fe_{65}Co_{10}B_{20}Si_1Zr_2Hf_2$, and (*f*) all alloys.

Table II. Magnetic Properties of Investigated Alloys

Alloy	H_C (A/m)	M_S (T)	D_{spf} (meV/nm^2)	T_C (K)	Crystalline Phases
$Fe_{65}Co_{11}B_{20}Zr_2Hf_2$	310	1.43	46	690	αFe + $Fe_{23}B_6$
$Fe_{65}Co_{10.75}B_{20}Si_{0.25}Zr_2Hf_2$	143	1.40	45	672	αFe + $Fe_{23}B_6$
$Fe_{65}Co_{10.5}B_{20}Si_{0.5}Zr_2Hf_2$	56	1.40	43	668	$Fe_{23}B_6$
$Fe_{65}Co_{10.25}B_{20}Si_{0.75}Zr_2Hf_2$	62	1.38	43	663	$Fe_{23}B_6$
$Fe_{65}Co_{10}B_{20}Si_1Zr_2Hf_2$	61	1.37	43	655	$Fe_{23}B_6$

determined of Si content on the crystallization temperature of the amorphous matrix (Figure 5).

In the solidified state, the diffusion of atoms is almost completely limited, and the tested state of the sample reflects accurately the effect of silicon on its properties. In the case of thermal processes during the measurement of magnetic polarization as a function of temperature, diffusion processes occur and the effect of silicon on the onset of the crystallization temperature of the amorphous matrix is reduced (Figure 5(a)). There is both chemical and topological disorder in amorphous materials. In contrast, only chemical disorder occurs in crystalline materials. In the heating process, up to a temperature of about 680 K, the magnetic saturation polarization process is affected by three phases: the amorphous phase and two crystalline phases. For alloys with the addition of Si, in this temperature range the course of thermomagnetic curves is very similar. Above this range, where the $Fe_{23}B_6$ phase becomes paramagnetic, the course of the curves is only related to the presence of the phase αFe (Figure 5(b)).

Figure 6 shows static magnetic hysteresis loops, measured in the range of external magnetic field up to 2T. The measured static magnetic hysteresis loops have a typical shape for magnetic materials exhibiting soft magnetic properties. The coercive field value, determined based on analysis of the hysteresis loops, falls within the range describing soft magnetic materials [36]

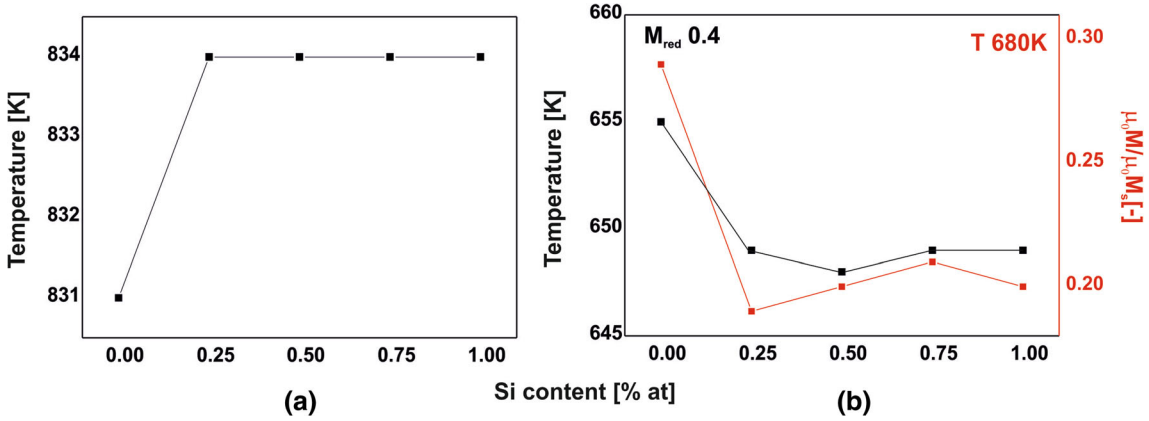

Fig. 5—Analysis of thermomagnetic curves: (*a*) onset of crystallization temperature of amorphous matrix, (*b*) assessment of the proportion of alloy crystallization.

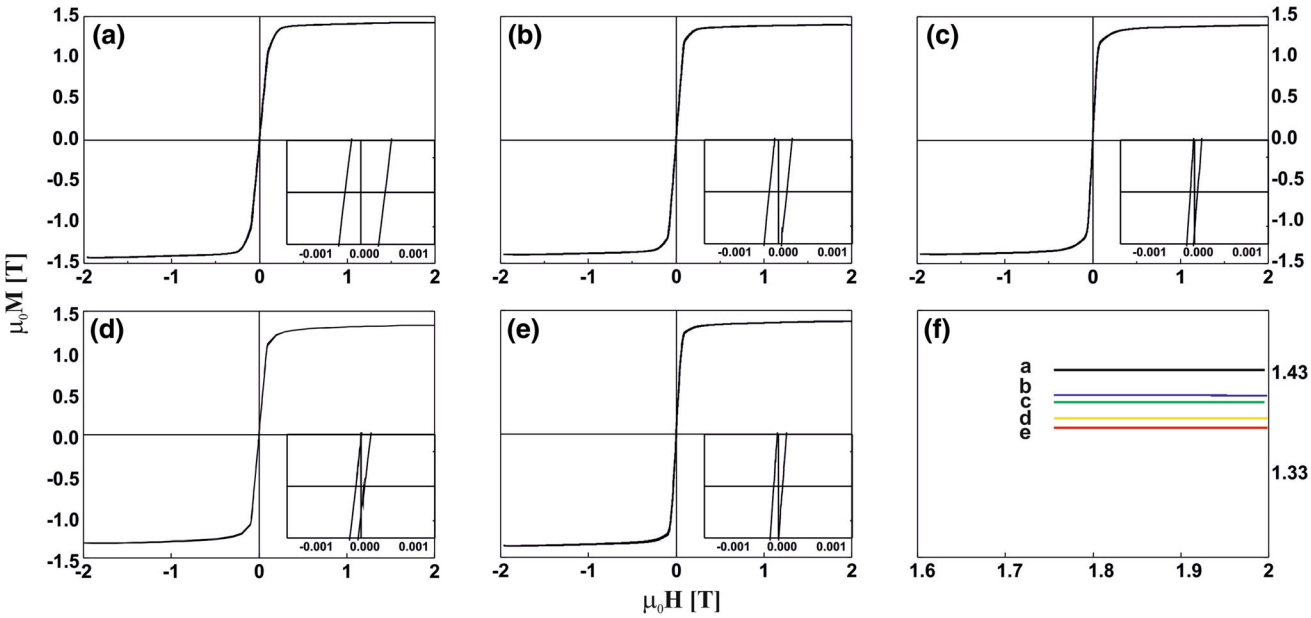

Fig. 6—Static magnetic hysteresis loops for the alloys: (*a*) $Fe_{65}Co_{11}B_{20}Zr_2Hf_2$, (*b*) $Fe_{65}Co_{10.75}B_{20}Si_{0.25}Zr_2Hf_2$, (*c*) $Fe_{65}Co_{10.5}B_{20}Si_{0.5}Zr_2Hf_2$, (*d*) $Fe_{65}Co_{10.25}B_{20}Si_{0.75}Zr_2Hf_2$, (*e*) $Fe_{65}Co_{10}B_{20}Si_1Zr_2Hf_2$, (*f*) saturation magnetization for tested alloys.

(Table II). It should be noted that the addition of Si reduced the coercive field value by more than 50 pct—from 310 to 143 A/m. For larger additions of Si, a reduction in the coercive field value was obtained—to a level of approximately 60 A/m. This means that the optimal Si content, of those tested in this work, is 0.5 at. pct. The investigated alloys are characterized by quite a high saturation magnetization around 1.4 T (Table II). The shape of the magnetization curves indicates that the tested materials did not have even a residual share of hard magnetic phases in their volume. In the first two alloys two crystalline phases αFe and $Fe_{23}B_6$ were observed. There was a much higher coercive field value for these alloys. For alloys with one $Fe_{23}B_6$ crystal phase, a significant decrease in the coercive field value was observed. The presence of the soft magnetic phase αFe in the volume of tested samples with an average grain size from 3 to 18 nm should ultimately affect the maximum magnetic softening of the material and give an ultra-soft magnetic material. Unfortunately, the presence of an additional magnetic phase—also magnetically soft, but with a much larger grain and high magnetic anisotropy [37]—makes it impossible to obtain a super-soft magnetic material. As demonstrated in Reference 38, borides significantly impede the free movement of domain walls. Even in the case where there is one magnetic phase—soft magnetic $Fe_{23}B_6$ with a small average grain—it was impossible to achieve significant magnetic softening.

Figure 7 presents high-field magnetization curves for the Holstein–Primakoff paraprocess.[39] Using Eq. [2], the value of the D_{spf} parameter was calculated. The highest value of this parameter was obtained for samples in which the αFe phase is present, *i.e.*,

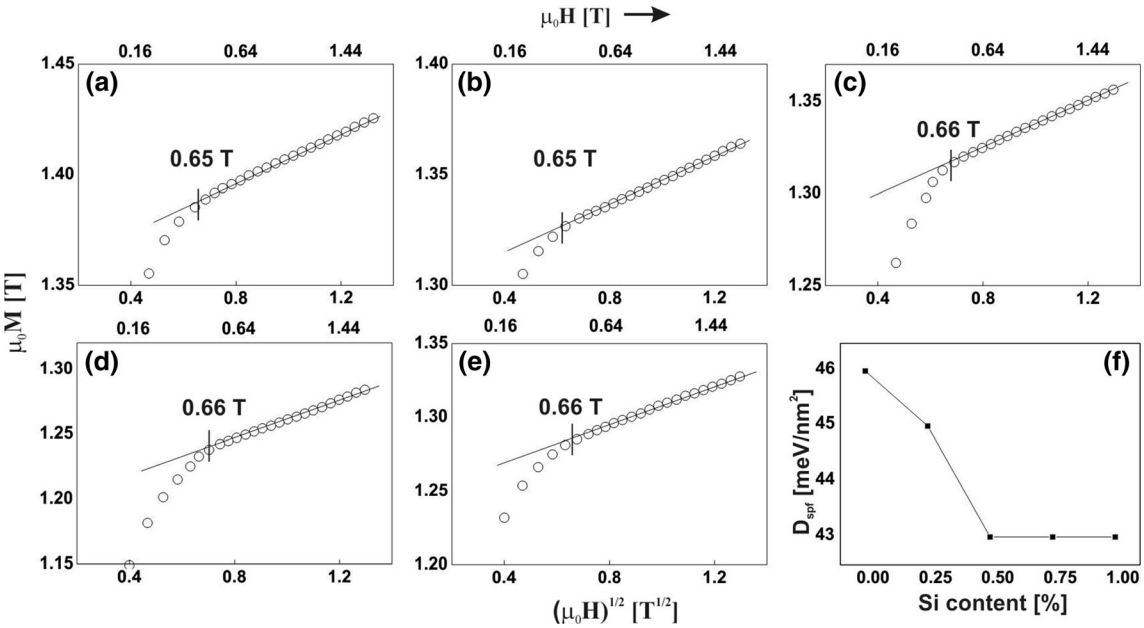

Fig. 7—Magnetization as a function of $(\mu_0 H)^{1/2}$ for the alloys: (*a*) $Fe_{65}Co_{11}B_{20}Zr_2Hf_2$, (*b*) $Fe_{65}Co_{10.75}B_{20}Si_{0.25}Zr_2Hf_2$, (*c*) $Fe_{65}Co_{10.5}B_{20}Si_{0.5}Zr_2Hf_2$, (*d*) $Fe_{65}Co_{10.25}B_{20}Si_{0.75}Zr_2Hf_2$, (*e*) $Fe_{65}Co_{10}B_{20}Si_1Zr_2Hf_2$, (*f*) dependence of the D_{spf} parameter on the Si content in the alloy.

$Fe_{65}Co_{11}B_{20}Zr_2Hf_2$ and $Fe_{65}Co_{10.75}B_{20}Si_{0.25}Zr_2Hf_2$. Changes in D_{spf} are associated with changes in the number of magnetic atoms in the immediate vicinity and the distance between them. A higher value of the spin-wave stiffness parameter indicates an increase in the number of magnetic atoms in the immediate vicinity, which is associated with the creation of long-range chemical and topological order. In addition, the value of the D_{spf} parameter will be affected by an amorphous matrix in which there is chemical and topological short-range disorder.[40] Changes in the short-range ordering are manifested as dampening re-arrangements of atoms in the long-range ordering, leading to stabilization of the supercooled liquid state (long-range order would be necessary for progress into the crystallization process).[41]

IV. CONCLUSIONS

This work examined the effect of silicon addition on the formation of nanocrystalline structure in the following rapidly-cooled alloys: $Fe_{65}Co_{11-x}B_{20}Si_xZr_2Hf_2$, where: x = 0; 0.25; 0.5; 0.75. Based on the tests performed, the following conclusions were made:

1. In the alloys with 0 and 0.25 at. pct content of Si, there were two crystalline phases: αFe and metastable $Fe_{23}B_6$. Borides hinder the free course of exchange interactions between αFe grains, which reduces effectively the expected value of the coercive field. The addition of 0.25 at. pct of Si resulted in the growth of αFe phase crystal grains. For an almost unchanged average grain size of the $Fe_{23}B_6$ crystalline phase, a 50 pct reduction was observed in the coercive field value. A slight change in saturation magnetization and Curie temperature were also observed for these samples;
2. For other samples (*i.e.*, addition of Si = 0.5; 0.75; 1), only borides were produced in the single-stage production process, for which the average grain size decreased with the Si content. It is interesting that, for samples containing only the $Fe_{23}B_6$ phase, a coercive field value was obtained which was more than five times lower than that for the samples containing the additional phase αFe. It should also be added that, even for small $Fe_{23}B_6$ phase grains, the coercive field value has not decreased, which would be expected;
3. Saturation magnetization for the tested samples was similar and was close to 1.4 T;
4. The onset of the crystallization temperature for the amorphous matrix is the same for all alloys with the addition of Si;
5. Analyzing the spin-wave stiffness parameter, it can be stated that the environment of magnetic atoms is the same for samples in which the αFe magnetic phase does not occur;
6. The lattice parameters for crystalline phases are reduced as the Si content in the alloy increases;
7. It can be stated that, for the alloys tested in this work, the Curie temperature decreases with Si content. It is possible that the presence of Si affects the lattice parameters and hence changes the exchange energy. This results in a decrease in the T_C value.

REFERENCES

1. H.R. Lashgari, D. Chua, S. Xie, H. Sun, M. Ferry, and S. Li: *J. Non. Cryst. Solids*, 2014, vol. 391, pp. 61–82.
2. D. Chu, H. Lashgari, Y. Jiang, M. Ferry, K. Laws, S. Xie, H. Sun, and S. Li: *Nanotechnol. Rev*, 2014, vol. 3, pp. 153–59.
3. B. Huang, Y. Yang, A.D. Wang, Q. Wang, and C.T. Liu: *Intermetallics*, 2017, vol. 84, pp. 74–81.
4. M. Ohta and Y. Yoshizawa: *J. Phys. D. Appl. Phys.*, 2011, vol. 44 (6), p. 064004.
5. J. Si, J. Mei, R. Wang, X. Chen, and X. Hui: *Mater. Lett.*, 2016, vol. 181, pp. 282–84.
6. G. Herzer: *Scripta Metall. Mater.*, 1995, vol. 33, pp. 1741–56.
7. Y. Geng, Z. Zhang, Z. Wang, Y. Wang, J. Qiang, C. Dong, H. Wang, and O. Tegus: *J. Non. Cryst. Solids*, 2016, vol. 450, pp. 1–5.
8. Y. Han, A. Inoue, F.L. Kong, C.T. Chang, S.L. Shu, E. Shalaan, and F. Al-Marzouki: *J. Alloys Compd.*, 2016, vol. 657, pp. 237–45.
9. G.T. Xia, Y.G. Wang, J. Dai, and Y.D. Dai: *J. Alloys Compd.*, 2017, vol. 690, pp. 281–86.
10. L. Zhang, Z. Wang, and Y. Jia: *Mater. Sci. Eng. B*, 2018, vol. 231, pp. 1–4.
11. L.Y. Guo, S.N. Geng, J. Pang, Y.H. Hu, S. Lan, C.M. Wang, and W.M. Wang: *Mater. Des.*, 2018, vol. 160, pp. 538–48.
12. T. Alam, T. Borkar, S.S. Joshi, S. Katakam, X. Chen, N.B. Dahotre, R.V. Ramanujan, and R. Banerjee: *J. Non. Cryst. Solids*, 2015, vol. 428, pp. 75–81.
13. S.F. Chen, C.Y. Hung, S.J. Wang, S.H. Chen, and C.C. Chen: *J. Alloys Compd.*, 2015, vol. 627, pp. 333–36.
14. K. Hono, D.H. Ping, M. Ohnuma, and H. Onodera: *Acta Mater.*, 1999, vol. 47 (3), pp. 997–1006.
15. H.J. Ma, J.T. Zhang, G.H. Li, W.X. Zhang, and W.M. Wang: *J. Alloys Compd.*, 2010, vol. 501 (2), pp. 227–32.
16. A. Inoue and B. Shen: *Mater. Sci. Eng. A*, 2004, vols. 375–377, pp. 302–06.
17. M. Nabiałek, B. Jeż, K. Błoch, P. Pietrusiewicz, and J. Gondro: *J. Magn. Magn. Mater.*, 2019, vol. 477, pp. 214–19.
18. M. Nabiałek: *J. Alloys Compd.*, 2015, vol. 642, pp. 98–103.
19. W. Zhang and A. Inoue: *Mater. Trans.*, 2001, vol. 42, pp. 1142–45.
20. M. Nabiałek, B. Jeż, and K. Jeż: *Revista de Chimie*, 2018, vol. 69 (9), pp. 2546–50.
21. A. Inoue, T. Zhang, and A. Takeuchi: *Appl. Phys. Lett.*, 1997, vol. 71, pp. 464–66.
22. Y. Wu, T. Bitoh, K. Hono, A. Makino, and A. Inoue: *Acta Mater.*, 2001, vol. 49 (19), pp. 4069–77.
23. K. Suzuki, A. Makino, A. Inoue, and T. Masumoto: *J. Appl. Phys.*, 1991, vol. 70 (10), pp. 6232–37.
24. L.H. Kong, Y.L. Gao, T.T. Song, G. Wang, and Q.J. Zhai: *Thermochim Acta*, 2011, vol. 522 (1), pp. 166–72.
25. A. Takeuchi and A. Inoue: *Mater. Trans.*, 2005, vol. 46 (12), pp. 2817–29.
26. J. Zhou, B. Sun, Q. Wang, Q. Yang, W. Yang, and B. Shen: *J. Alloys Compd.*, 2019, vol. 783, pp. 555–64.
27. B. Jeż: *Rev. Chim.*, 2017, vol. 68 (8), pp. 1903–07.
28. E.S. Park, H.K. Lim, W.T. Kim, and D.H. Kim: *J. Non. Cryst. Solids*, 2002, vol. 298, pp. 15–22.
29. O. Kohmoto: *J. Appl. Phys.*, 1982, vol. 53, p. 7486.
30. J. Xu, Y. Yang, W. Li, Z. Xie, and X. Chen: *Mater. Res. Bull.*, 2018, vol. 97, pp. 452–56.
31. M.E. McHenry, M.A. Willard, and D.E. Laughlin: *Prog. Mater. Sci.*, 1999, vol. 44, p. 291.
32. A. Inoue, B. Shen, and A. Takeuchi: *Mater. Sci. Eng. A*, 2006, vol. 441, pp. 18–25.
33. J.M. Borrego, C.F. Conde, and A. Conde: *Phil. Mag. Lett.*, 2000, vol. 80, pp. 359–65.
34. G. Herzer: *IEEE Trans. Magn.*, 1990, vol. 26 (5), pp. 1397–402.
35. G. Herzer: *Handb. Magn. Mater.*, 1997, vol. 10, pp. 415–62.
36. H. Liebermann: *Rapidly Solidified Alloys*, Springer, New Jersey, 1993.
37. Y.-G. Park, H.S. Park, D. Shindo, and Y. Yoshizawa: *Mater. Trans.*, 2005, vol. 46, pp. 3059–62.
38. A.-T. Le, C.-O. Kim, N. Chau, N.D. Cuong, N.D. Tho, N.Q. Hoa, and H. Lee: *J. Magn. Magn. Mater.*, 2006, vol. 307, pp. 178–85.
39. T. Holstein and H. Primakoff: *Phys. Rev.*, 1941, vol. 59, pp. 388–94.
40. N. Lenge and H. Kronmüller: *Phys. Stat. Sol. (a)*, 1986, vol. 95, pp. 621–33.
41. Z. Long, Y. Shao, F. Xu, H. Wei, Z. Zhang, P. Zhang, and X. Su: *Mater. Sci. Eng.*, 2009, vol. 164, pp. 1–5.